Am(III) coprecipitation with and adsorption on the smectite hectorite

N. Finck *, K. Dardenne, H. Geckeis

Institute for Nuclear Waste Disposal (INE), Karlsruhe Institute of Technology (KIT), P.O. Box 3640, D-76021 Karlsruhe, Germany

ARTICLE INFO

Keywords:
Smectite
Americium
Coprecipitation
Adsorption
EXAFS spectroscopy

ABSTRACT

Clay minerals, such as the smectite hectorite, have been detected in the alteration layer of nuclear waste glass corroded in laboratory experiments. The neoformation of such secondary phases upon dissolution and re precipitation represents a significant retention potential for radionuclide released during the waste matrix alteration.

Hectorite was synthesized from a brucite precursor phase in the presence of trivalent americium, and separately, the Am(III) aqua ions were adsorbed on the smectite in order to decipher the actual retention mechanism(s). X ray diffractograms indicated that both brucite and hectorite formed and that the actinide had no significant influence on the syntheses. No separate phase was detected by XRD and no Am containing precipitate was detected by SEM EDX. The Am local chemical environment was probed by EXAFS spectroscopy. In the precursor, the polarized EXAFS data are consistent with Am(III) very likely substituting for Mg at octahedral site. The weak angular dependence on the data and the split nearest octahedral neighboring shell suggest that the substitution significantly distorts the local brucite structure. In hectorite, americium is 6 fold coordinated by oxygen atoms and next nearest Mg and Si shells are detect ed at distances strongly pointing to an octahedral clay like environment. EXAFS data of the actinide adsorbed onto hectorite are consistent with the formation of monomeric inner sphere surface complexes at the platelet edges. The formation of Am(III) surface complexes during the coprecipitation experiment is marginal.

The results show that clay minerals synthesized under controlled conditions can accommodate trivalent actinides, and thus lanthanides, at octahedral position within the structure. The identified retention mechanism can in principle be applied to all sheet silicates, including those occurring in nature and for which no such structural investigation has been reported.

1. Introduction

Smectites, such as the Al rich montmorillonite, are constituents of bentonites and confer to these materials cost efficient hydraulic and chemical properties. Bentonites are widely used in remediation technologies for the isolation of pollutants. For example, these materials find application as liners and capping layers in the disposal of municipal and industrial wastes and could be used as backfill in deep HLW repositories (Gates et al., 2009). Smectites are phyllosilicates made of two tetrahedral sheets (mostly containing Si) apart from one octahedral sheet (mostly containing Al or Mg). Isomorphic substitution within the structure (e.g., Al for Si, Mg for Al, or Li for Mg) generates an excess negative charge which is balanced by cations adsorbed on basal planes. Smectites are known to be highly reactive with respect to cations in aqueous systems. Cations can interact with negatively charged surfaces by purely electrostatic attraction and they can also be strongly bound to the surface and involve a chemical bonding. The adsorption of cations onto smectites was extensively studied in the past and surface complexation models could be developed on the basis of a molecular scale process understanding (e.g., (Bradbury and Baeyens, 2002)). The most efficient immobilization, however, may consist in cations incorporated within the structure of smectite.

Clay minerals may play an important role in the safe disposal of nuclear waste. Several countries operating nuclear power plants have decided to reprocess their spent fuel and to vitrify the resulting high level wastes (HLW). This HLW glass is foreseen to be disposed of in deep geological repositories (e.g., in a clay host rock) to isolate it from the geosphere. In such facilities, groundwater will very likely move through the engineered barriers made of e.g., bentonite and come in contact with the glass over the geological time scales needed to reduce the radiotoxicity of these wastes. In aqueous environments, a reaction layer will form at the surface of the glass, followed by an alter ation layer. Various neoformed secondary phases have been identified in the alteration layer of glass corroded in laboratory experiments, such as powellite and sheet silicates (Zimmer et al., 2002; Jollivet et al., 2012). The formation of such phases represents a significant re tention potential for long lived and radiotoxic radionuclides (RN),

* Corresponding author. Tel.: +49 721 6082 4321.
E-mail address: nicolas.finck@kit.edu (N. Finck).

including the actinides (An), that will be released upon waste matrix corrosion. Specifically, the magnesian smectite hectorite ($Na_{0.33}[Li_{0.33}Mg_{2.67}Si_4O_{10}(OH)_2]$) has been detected in corrosion experiments by clayey water of simulated nuclear waste glass (Jollivet et al., 2012).

Under the reducing conditions expected to develop in clay based repositories (Gaucher et al., 2006), the actinides Cm, Am and some Pu may occur as trivalent cations. The ionic radii of these elements 6 fold coordinated by oxygen ($r^{VI}(Cm(III)) = 0.97$ Å, $r^{VI}(Am(III)) = 0.98$ Å, $r^{VI}(Pu(III)) = 1.00$ Å) are larger than those of major cations typically present in clay octahedral sheets (e.g., $r^{VI}(Mg(II)) = 0.72$ Å, $r^{VI}(Li(I)) = 0.76$ Å, $r^{VI}(Fe(II)) = 0.78$ Å) (Shannon, 1976). Although some incorporation of An(III) at octahedral sites cannot be excluded from the difference in sizes, the structural retention may be limited/hindered by large structural strain. Based on crystal chemistry, octahedra exist for ionic radius of cation (r_C) to ionic radius of anion (r_A) ratios of between 0.414 and 0.732 (Pauling, 1929). Consequently, actinides ($0.69 < r_C/r_A < 0.71$) can in principle substitute for cations typically present at clay octahedral sites.

Structural substitution within the octahedral sheet of clay minerals in nature has been known for many decades (Brindley & Brown 1980). More specifically, the concentration of lanthanides (Lns) in sedimentary clay minerals can provide indications of possible incorporation mechanisms. For example, Severmann et al. (2004) investigated the origin of hydrothermally formed nontronite (an Fe rich smectite). They reported an enrichment in heavy (i.e., smaller) Ln(III) compared to the lighter ones, and data were consistent with incorporation via coprecipitation and an uptake governed by crystal chemistry. The methodology used to prepare the samples ensured that the measured Ln contents reflected lattice bound cations rather than adsorbed species. However, no spectroscopic technique was used to directly characterize the Ln species in such natural samples. Clay minerals can also be synthesized in the laboratory under controlled conditions. Syntheses of the magnesian smectite hectorite in the presence of An(III) or Ln(III) (used as non radioactive chemical surrogates of actinides) have been reported. Luminescence data collected for hectorite crystallized in the presence of Cm(III) (Brandt et al., 2007) or Eu(III) (Finck et al., 2008) were consistent with incorporation in the bulk structure. Recent X ray absorption spectroscopy (XAS) data also showed the possibility of incorporating Lu(III) in the octahedral sheet of hectorite (Finck et al., 2009). However, structural data (i.e., coordination numbers and bond lengths) needed to assess the actual structural retention mechanism are still lacking for the actinides. Understanding the mechanism of structural incorporation of trivalent *f* elements (actinides or lanthanides) under controlled conditions in the laboratory will in principle be applicable to almost all sheet silicates.

In the present study, the Am(III) retention mechanism(s) upon coprecipitation with or adsorption on hectorite were investigated. In the coprecipitation experiments, hectorite was crystallized from a brucite precursor that was synthesized in the presence of Am(III). In the adsorption experiment, the Am(III) ions contacted pre formed hectorite. The solid phases were characterized by X ray diffraction (XRD) and by scanning electron microscopy (SEM). Information on the americium chemical environment was obtained by probing the Am L_3 edge by extended X ray absorption fine structure (EXAFS) spectroscopy. This is the first study to report structural data on coprecipitation of a trivalent actinide with clay minerals using EXAFS spectroscopy.

2. Experimental

2.1. Sample preparation

All samples were prepared with ultra pure water (18.2 MΩ/cm, Milli Q system) and reagents of ACS grade or higher. The acidic Am(III) stock solutions contained 17 mmol/L ^{243}Am and 0.6 mmol/L ^{241}Am in nitrate medium in the coprecipitation experiments, and 11 mmol/L ^{243}Am and 0.4 mmol/L ^{241}Am in perchloric medium (the stock solution in perchloric medium is thereafter named sample $Am(III)_{aq}$) in the adsorption experiment. Hectorite (sample Hec) was synthesized from a freshly precipitated and washed brucite ($Mg(OH)_2$) precursor phase that was aged in the presence of LiF and silica sol for 2 days at 100 °C (Finck et al., 2009). After synthesis, the hectorite was washed at pH ~3 to remove any remaining precursor phase. In the Am coprecipitation experiment (sample AmCopHec), part of the magnesium was replaced by americium and the synthesis protocol was adapted as follows. The freshly precipitated and washed Am containing brucite was aged in the presence of the reactants (LiF, silica sol) for 6 days at 90 °C (Brandt et al., 2007) in a tightly closed Teflon inner coated vessel. After synthesis, AmCopHec was also washed at pH ~3 prior to further analyses. Separately, an Am containing brucite phase (sample AmCopBru) was prepared under identical conditions as described above. In the adsorption experiment, $Am(III)_{aq}$ was adsorbed on Hec (sample AmAdsHec) using a mass of 2 g/L, $[Am(III)]_{tot} = 105$ μmol/L, pH = 6.4 ± 0.1 (thereafter the condensed notation 6.4(1) is used for uncertainties), $I = 0.5$ mol/L $NaClO_4$, and 2 days contact time. This time was shown to be sufficient to reach equilibrium, e.g., (Bradbury and Baeyens, 2002; Rabung et al., 2005). ICP MS measurements indicated that 66% of the initial Am was adsorbed at the hectorite surface. AmCopBru and AmAdsHec were used as reference compounds. AmCopBru was prepared as an oriented sample by slow filtration of the suspension in order to collect polarized EXAFS data. Part of the AmCopBru and AmCopHec were dissolved in acidic medium and the solutions were analyzed by ICP MS (PerkinElmer ELAN 6100). The determined Mg:Am molar ratios in AmCopBru and AmCopHec are 335:1 and 1077:1, respectively. These data indicate that part of the Am was released from the precursor during the hectorite crystallization.

All solid phases were characterized by powder X ray diffraction (XRD) on oriented samples. The diffractograms were collected with a D8 Advance (Bruker) diffractometer (Cu K_α radiation) equipped with an energy dispersive detector (Sol X). The phase identification was performed by comparison with the PDF 2 database using the DIFFRAC.EVA 3.0 software (Bruker) and fits to the data were provided by the TOPAS 4.2 software (Bruker). The samples were also analyzed by scanning electron microscopy (SEM) with a CamScan CS44FE microscope (morphology) and elemental information was provided by energy dispersive X ray (EDX) spectroscopy.

2.2. X ray absorption spectroscopy

Americium L_3 edge EXAFS spectra were collected at the INE Beamline (Rothe et al., 2012) for actinide research at ANKA (Germany) with a storage ring energy of 2.5 GeV and a ring current of 90 170 mA. The energy calibration was done by setting the *K* edge of a Nb foil at 18,986 eV and this reference was measured along with all samples. The spectra were collected in fluorescence yield detection mode using a silicon drift detector (Vortex, SII NanoTechnology). Powder EXAFS data were collected for $Am(III)_{aq}$, AmCopHec and AmAdsHec and polarized EXAFS (P EXAFS) data were collected for AmCopBru at angles (α) between the layer plane of brucite and the electric field of the X ray beam of 10°, 35° and 80°. In a P EXAFS experiment, neighboring backscatterers located in plane are probed preferentially at α = 10° whereas the contributions from out of plane shells are weakened. The opposite trend is observed at 80°. Finally, polarized and powder EXAFS data are identical at α = 35° (Schlegel et al., 1999b). Data analysis was performed following standard procedures by using Athena and Artemis interfaces to Ifeffit software (Ravel and Newville, 2005). The EXAFS spectra were extracted from the raw data and Fourier transforms (FTs) were obtained from the $k^3 \times \chi(k)$ functions. Data fitting was performed in *R* space using a single scattering approach. For each coordination shell, phase and

amplitude functions of each scattering path (i.e., absorber and backscatterer atomic pair) were calculated separately with feff8.4 (Ankudinov et al., 1998) and the fit was provided by using combinations of single paths. The amplitude reduction factor (S_0^2) was set to 0.88. The P EXAFS data were modeled simultaneously at all angles using a common value for ΔE, and for a given shell, a common bond length and mean square displacement (or Debye Waller factor) taking into account the thermal and the structural disorder. The uncertainties on EXAFS distances are typically ± 0.02 Å for well resolved atomic shells and $\pm 20\%$ on the coordination numbers. The experimental uncertainty on α is estimated to $\pm 1°$. The fit quality was quantified by the R_f factor representing the absolute misfit between theory and experimental data (see Appendix).

3. Results and discussion

3.1. X ray diffraction and scanning electron microscopy

The powder X ray diffractograms of AmCopBru, Hec and AmCopHec are shown in Fig. 1. AmCopBru was identified as brucite and no other (crystalline) phase was detected. A good fit to the data was produced using the structure of brucite (Catti et al., 1995) in which Am replaces part of the Mg (molar ratio Mg:Am = 335:1) at octahedral sites. The lattice parameters in AmCopBru ($a = 3.14689(23)$ Å, $c = 4.77506(23)$ Å) differ only marginally from those reported for $Mg(OH)_2$ ($a = 3.1498(0)$ Å, $c = 4.7702(1)$ Å) (Catti et al., 1995). This result indicates that Am had no influence on the brucite precipitation and that the actinide only marginally affects the lattice constants, consistent with the low content. The diffractograms of Hec and AmCopHec are identical and typical of smectite. The basal spacing of $d(001) \sim 15.2(1)$ Å is typical of smectite with two interlayer hydration water molecules (Meunier, 2005). There is no evidence of any other separate phase on the diffractograms.

The SEM micrographs (Fig. 2) suggest that all three solid phases have a layered structure. This is consistent with the crystal habit of brucite (AmCopBru) and hectorite (Hec and AmCopHec). The micrographs of AmCopBru demonstrate the successful preparation as an oriented sample. They also indicate that it consists of aggregates of smaller particles of up to 200 300 nm in size. The micrographs of Hec and AmCopHec also indicate the presence of aggregates of particles of 200 to 500 nm in size. The particles are of similar disc like morphology in both samples, indicating that neither Am(III) influenced the clay synthesis (shape and type of sample), nor did the lower synthesis temperature of AmCopHec (90 °C) compared to Hec (100 °C).

SEM EDX spectra were recorded at several positions on AmCopBru. No local high Am content could be detected, consistent with the absence of X ray amorphous Am containing precipitate. This suggests that the actinide is very likely dispersed within the sample. Element maps (SEM EDX) were recorded for AmCopHec and AmAdsHec for Mg, Si and Am (Fig. 2). Mg and Si data are nicely correlated, consistent with expectations for signatures of the bulk material. This also excludes the presence of X ray amorphous silica. Americium is also homogeneously distributed in AmCopHec; no local accumulation as X ray amorphous Am containing precipitate can be seen. The data also show that Am is homogeneously distributed in AmAdsHec with, however, some areas of higher content (Fig. 2). These local accumulations can best be explained by the properties of the substrate. The micrograph indicates that Hec contains aggregates composed of particles of various sizes. Smaller particles have larger surfaces available for adsorption compared to larger particles so that the local higher Am contents may best be explained by higher retention at the surface of aggregates composed of small particles.

3.2. X ray absorption spectroscopy

3.2.1. Americium coprecipitated brucite

The Am(III) local chemical environment in AmCopBru was probed by P EXAFS spectroscopy. First, the spectrum of $Am(III)_{aq}$ (Fig. 3) displays a single wave frequency with monotonically decreasing amplitude, consistent with a single ordered coordination sphere. The data were fit with a single oxygen shell at $R_{Am-O1} = 2.47(2)$ Å containing $N_{O1} = 9.0$ atoms (Table 1), consistent with reported data (Skerencak Frech et al., 2014).

Upon coprecipitation with brucite, the Am(III) chemical environ ment changed. This is indicated by the reduction in amplitude of the EXAFS oscillations and the appearance of spectral features at $k > 8$ Å^{-1} (Fig. 3). Compared to $Am(III)_{aq}$, the amplitude of the first contribution in the Fourier transform is reduced and a contribution can be seen at

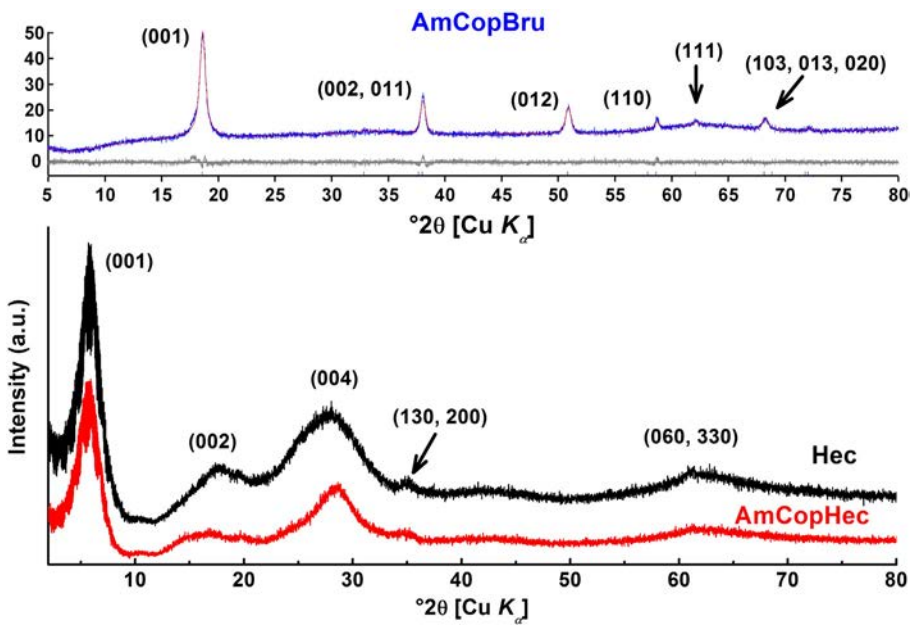

Fig. 1. Experimental (blue) and modeled (red) X-ray diffractogram of the sample AmCopBru (upper), the grey line represents the difference between the experimental and the modeled data. X-ray diffractograms of samples Hec and AmCopHec (lower). The numbers in parentheses indicate the lattice planes. (For interpretation of the references to color in this figure legend, the reader is referred to the web version of this article.)

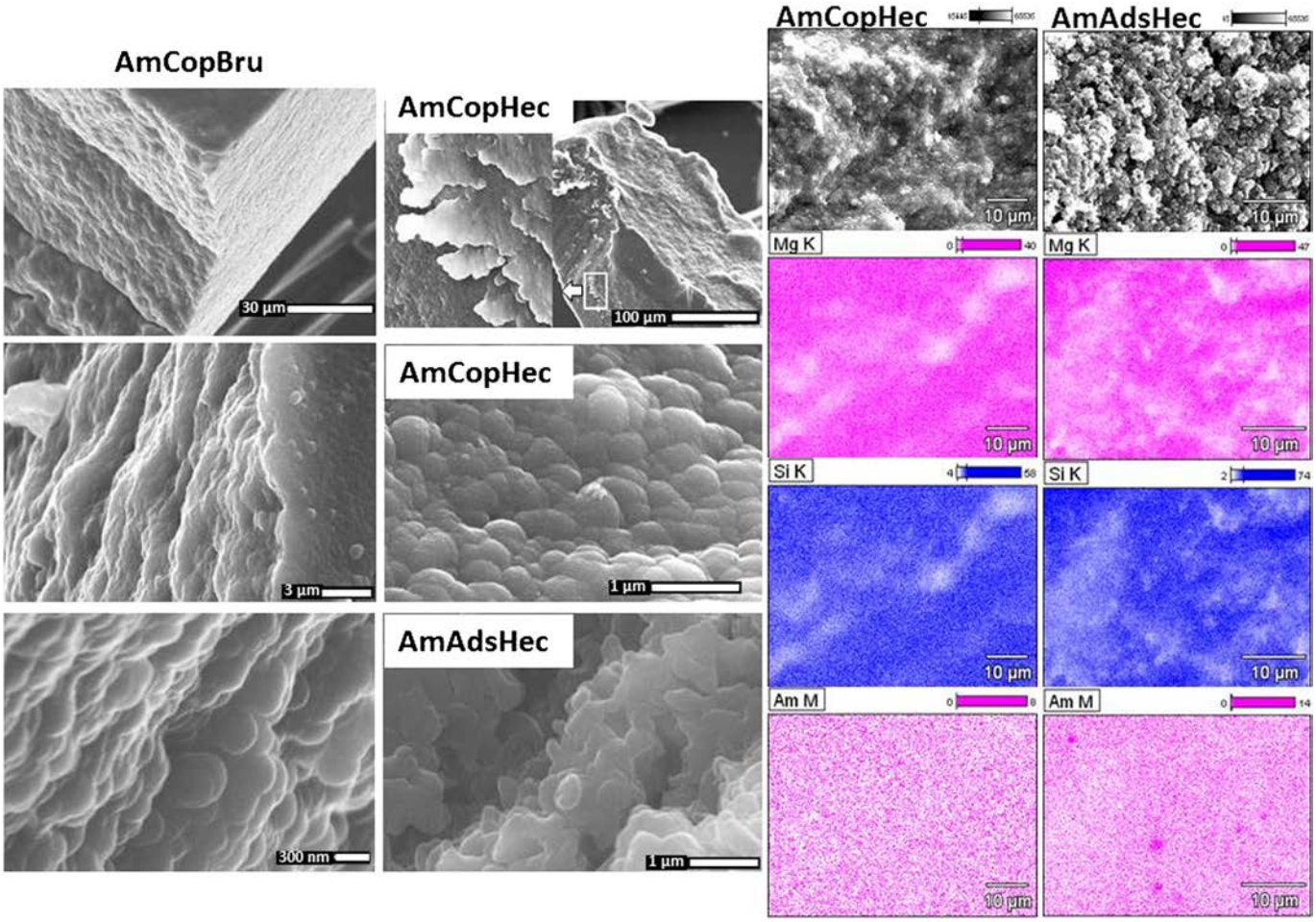

Fig. 2. SEM micrographs of AmCopBru, AmCopHec and AmAdsHec, and elemental maps obtained by energy-dispersive X–ray spectroscopy for AmCopHec and AmAdsHec.

$R + \Delta R \sim 3\ 4$ Å. The P EXAFS spectra display only very weak angular de pendences (Fig. 4). Accordingly, the FTs are also only weakly affected by a change in α: the amplitude of the first FT contribution slightly decreases with increasing angle, and the contribution at $R + \Delta R \sim 3$ 4 Å does not exhibit a clear angular dependence.

The FT contribution at $R + \Delta R \sim 2$ Å could be fit with a single O shell at $R_{Am-O1} = 2.44(1)$ Å containing $N_{O1} = 6.2$ atoms (Table 1). The apparent coordination number of this shell slightly decreases with increasing angle, hinting an in plane orientation as could be expected for brucite. However, the magnitude of the variation is close to uncertainties. Higher distance contributions were modeled by considering Mg ($R_{Am-Mg1} = 3.24$ Å and $R_{Am-Mg2} = 3.48$ Å) and O shells ($R_{Am-O2} = 3.87$ Å and $R_{Am-O3} = 4.38(2)$ Å) (Table 2). The Mg1 and Mg2 shells are separated by only 0.24 Å, suggesting that it may in fact correspond to a single Mg shell located approximately at $R_{Am-Mg} = (3.24 + 3.48) / 2 = 3.36$ Å and split into two subshells. Both Mg subshells exhibit no polarization dependence, possibly as a consequence of mutual extinction of their contributions. Finally, two O shells were used to model higher distance contributions. No Am backscatterer was detected, ruling out the precipitation of an Am containing precipitate, which is consistent with the SEM EDX results.

The Am first coordination sphere is consistent with an octahedral environment. However, the strain induced by the Am structural retention leads to a split in the neighboring Mg shell, which is pulled away from regular positions either in plane and/or out of plane. Obviously, brucite accommodated Am at octahedral sites but at the expense of the structure, as anticipated from the size mismatch. As a consequence, this structural disorder drastically reduced the angular dependence of the O1 shell and extinguished the dependence of the Mg1 and Mg2 shells. The actinide is thus not located in a well defined anisotropic environment but rather in a series of slightly differing environments and the sum of their contributions weakens any angular dependence. Additionally, considering the increase in size (Shannon, 1976) from Mg to Am (0.26 Å) and $R_{Mg-Mg} = 3.15$ Å in brucite (Catti et al., 1995), the calculated R_{Am-Mg} bond length ($3.15 + 0.26 = 3.41$ Å) is very close to the experimental mean value obtained from the Mg1 and Mg2 shells, corroborating the presence of Am in the bulk brucite. The calculated value corresponds to a planar geometry and thus the experimental bond length may possibly correspond to polyhe dra binding in a slightly bent geometry. The findings indicate that the actinide is located in a brucite like environment and that only a marginal amount, if at all, is located at the surface.

3.2.2. Americium coprecipitated hectorite

The crystallization of AmCopHec from AmCopBru proceeds by condensation of two tetrahedral sheets onto the brucite octahedral sheet. During that reaction, the Am local chemical environment further changed. In the EXAFS spectrum, the amplitude of the oscillations is reduced and the frequencies are slightly changed compared to the precursor phase (Fig. 3). In the FT, the amplitude of the first peak is lower and the contributions at higher distances are clearly different.

The spectral simulation indicates that the Am(III) first coordination sphere consists of a single oxygen shell located at $R_{Am-O1} = 2.43(1)$ Å containing $N_{O1} = 5.8$ atoms (Table 1). Both R_{Am-O1} and N_{O1} are consis tent with Am(III) hexacoordinated by O atoms. Higher distance contri butions were modeled with one Mg ($R_{Am-Mg1} = 3.17$ Å) and one Si ($R_{Am-Si1} = 3.33(3)$ Å) shell, and possibly one O shell at $R_{Am-O2} = 3.71$ Å (Table 2). The O1 shell is located at the same distance, within

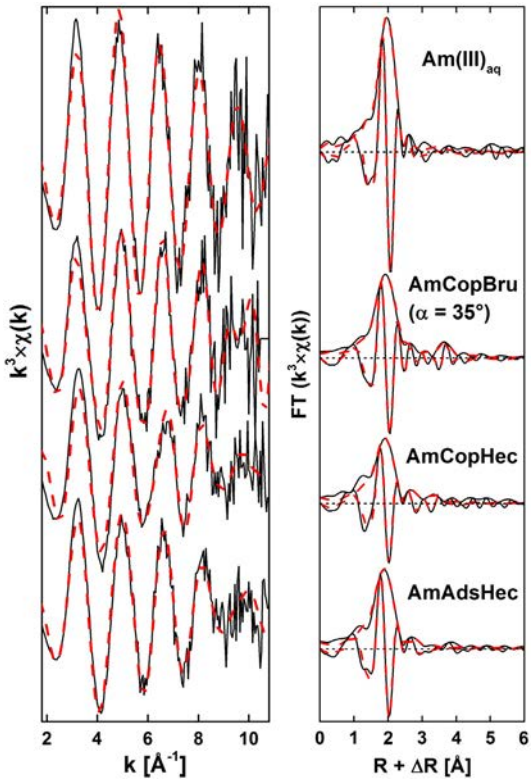

Fig. 3. Experimental (solid black) and modeled (red dash) powder EXAFS spectra (left) with the corresponding Fourier transforms (right). The fit results are given in Tables 1 and 2. (For interpretation of the references to color in this figure legend, the reader is referred to the web version of this article.)

the uncertainty, as in AmCopBru, implying that the octahedral environment was kept during the hectorite crystallization. Only one Mg shell is detected in AmCopHec, contrary to AmCopBru, and R_{Am-Mg1} is slightly shorter in the doped hectorite. The environment corresponding to the Mg2 shell in AmCopBru was thus less stable and leads to a release of the actinide. This conclusion is consistent with the decrease in Am content from AmCopBru to AmCopHec observed by chemical analysis of the solids.

The results indicate that Am is located in an octahedral environment, with Mg and Si shells at distances typical of clay like environments. R_{Am-Mg1} and R_{Am-Si1} in AmCopHec are larger than R_{Mg-Mg} ($R_{Mg-Mg} = 3.04$ Å (Seidl and Breu, 2005)) and R_{Mg-Si} ($R_{Mg-Si} = 3.25$ Å (Seidl and Breu, 2005)) in hectorite, respectively, but the increase in bond length due to the substitution is smaller than the increase in ionic radius. Furthermore, the distance between adjacent octahedral cations decreases from brucite ($R_{Mg-Mg} = 3.15$ Å) to hectorite ($R_{Mg-Mg} = 3.04$ Å (Seidl and Breu, 2005)) and the same trend was observed from AmCopBru ($R_{Am-Mg1} = 3.24$ Å) to AmCopHec ($R_{Am-Mg1} = 3.17$ Å). These results add further evidence of an accommodation of Am in the bulk hectorite.

The number of detected Mg backscatterers is lower in AmCopHec than in AmCopBru. The decrease in R_{Mg-Mg} from brucite to hectorite goes along with a decrease in the size of the octahedral sites. These sites are thus less able to accommodate larger cations such as actinides. In AmCopBru, next nearest cations could be pulled away in plane/out of plane because the structure made of only octahedral sheets is more flexible than the rigid hectorite layers made of tetrahedral octahedral tetrahedral sheets. Consequently, Am occupies a highly strained clay like octahedral environment, as indicated by the larger mean square displacement factors in AmCopHec (for example $\sigma^2 = 0.011$ Å^2 for the O1 shell) compared to AmCopBru ($\sigma^2 = 0.008$ Å^2 for the O1 shell), resulting in a certain distribution of interatomic distances around a mean value. This dampens the EXAFS oscillatory contribution from the Mg1 shell, leading to a low number of detected atoms. Additionally, Li(I) may be co incorporated in adjacent octahedral sites for local charge balance and lithium is too light to be detected by EXAFS spectroscopy, reducing the number of detected octahedral neighbors. The structural strain may also very likely influence the condensation of the tetrahedral sheets onto the octahedral sheet. In the vicinity of the actinide, the tetrahedral sheets certainly did not condense as well and properly as in hectorite, leading to Si atoms located at larger distances in AmCopHec ($R_{Am-Si1} = 3.33$ Å) than in hectorite ($R_{Mg-Si} = 3.25$ Å (Seidl and Breu, 2005)) and to a lower number of detected Si1 atoms. Finally, no Am backscatterer was detected, ruling out the precipitation of any separate Am containing phase and correlating with the findings from the SEM EDX analysis.

The present results suggest that Am is located in a highly strained clay like octahedral environment in AmCopHec. According to the synthesis protocol, this can only result from an incorporation during crystal growth. Americium is taken up structurally in the brucite octahedral layer (AmCopBru) and remains at its structural site, at least part of it, during the clay crystallization (AmCopHec).

3.2.3. Americium adsorbed on hectorite

Americium can only be retained at the surface of hectorite in AmAdsHec and the comparison of the data of this sample with that of AmCopHec will further strengthen the conclusion of a structural retention in the coprecipitation sample. The spectrum of AmAdsHec differs in amplitude ($5 < k < 8$ Å^{-1}) and slightly in position of the frequency maxima compared to that of AmCopHec (Fig. 3), indicating distinct crystal chemical environments. This is also seen on the corresponding FTs where the position, the amplitude and the phase of the contributions differ at $R + \Delta R > 2.5$ Å. The spectral simulation indicates that Am(III) is bound to $N_{O1} = 7.2(3)$ atoms located at $R_{Am-O1} = 2.42$ Å in the first coordination sphere (Table 2). Next nearest neighbors consist of Mg and Si shells located at $R_{Am-Mg1} = 3.22$ Å and $R_{Am-Si1} = 3.38$ Å, and possibly one O shell at $R_{Am-O2} = 3.79$ Å (Table 2). No Am backscatterer

Table 1
Quantitative EXAFS analysis of the first FT peak of all samples[a].

Sample	Angle (α)	FT range[b] [Å^{-1}]	Fit range[c] [Å]	O1 shell			ΔE_0	R_f
				N	R	σ^2		
Am(III)$_{aq}$	35°	3.2–10.1	1.7–2.7	9.0	2.47(2)	0.008	1.4(7)	0.0051
AmCopBru	10°	3.2–9.0		6.5				
	35°	3.2–9.1	1.6–4.5	6.2	2.44(1)	0.008	1.8(4)	0.0095
	80°	3.2–9.1		5.7				
AmCopHec	35°	3.3–9.7	1.5–4.2	5.8	2.43(1)	0.011	3.1(9)	0.0127
AmAdsHec	35°	3.3–9.7	1.5–4.2	7.2(3)	2.42	0.011	0.6(1.1)	0.0051

N is the coordination number, R is the interatomic distance [Å], σ^2 is the mean square displacement [Å^2], ΔE_0 is the shift in ionization energy [eV] with E_0 threshold energy taken as maximum of first derivative, and R_f is the figure of merit of the fit. The number in parentheses indicates the uncertainty, otherwise parameter held fixed.

[a] The data were fit over the entire range considering all shells from Tables 1 and 2.

[b] Fourier transformed range.

[c] $R + \Delta R$ interval for the fit.

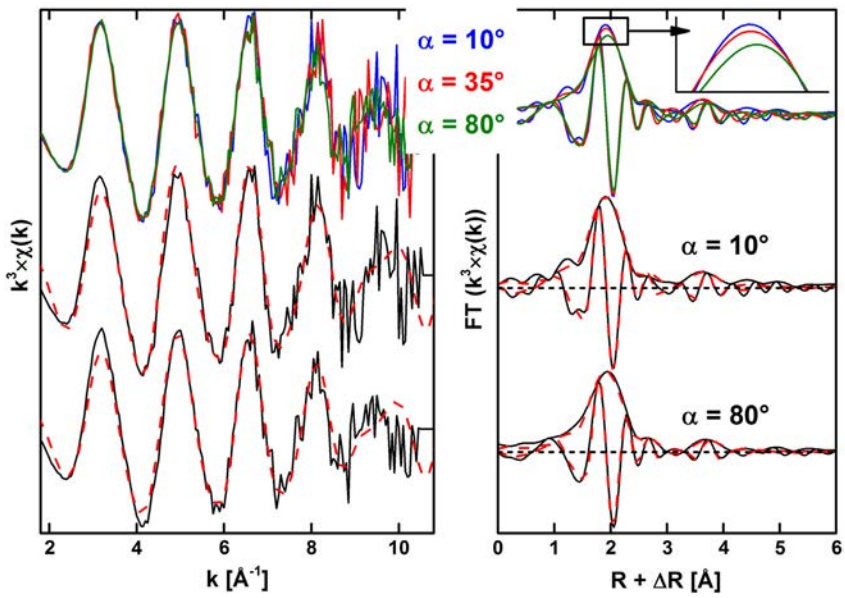

Fig. 4. Polarized EXAFS spectra (left) and the corresponding Fourier transforms (right) of AmCopBru. The fit results are given in Tables 1 and 2.

could be detected, ruling out the formation of polymeric species or of X ray amorphous precipitate. This finding corroborates the hypothesis of a local accumulation at the surface as a consequence of small particle sizes evidenced by SEM.

From the aqua ions (sample $Am(III)_{aq}$) to AmAdsHec, the reduction in N_{O1} indicates a significant change in the chemical environment upon interaction with the clay surface. The formation of outer sphere surface complexes can be excluded because Am would have kept its entire hydration sphere (9 neighboring O atoms located at the same distance as $Am(III)_{aq}$). Obviously, the Am first coordination sphere changed because $N_{O1} = 7.2(3)$ and $R_{Am-O1} = 2.42$ Å are lower and shorter, respectively, than in $Am(III)_{aq,}$ and at the same time the mean square displacement factor increased. This latter indicates slight variations in the Am—O distances leading to destructive interferences of EXAFS oscillations having small differences in their amplitude (Stumpf et al., 2004). For example, it can originate from the simultaneous existence of slightly different surface complex structures at the mineral surface (Polly et al., 2010). Yet, only one single shell was detected at $R_{Am-O1} = 2.42$ Å and can best be explained as the sum of contributions from surface oxygens (two) and from hydration water oxygens (five as usually reported e.g., (Stumpf et al., 2004)). The O1 shell coordination number in AmCopHec is significantly lower ($N_{O1} = 5.8$) than in AmAdsHec ($N_{O1} = 7.2(3)$), indicating that the crystal chemical environments are dissimilar. This result thus implies that Am is not predominantly surface retained in AmCopHec but occluded in the bulk upon coprecipitation with hectorite.

Mg and Si neighbors were detected at slightly larger distances in AmAdsHec than in AmCopHec. These results indicate that Am binds to Mg octahedra at the platelet edges where they are exposed and not to Si units. This further excludes a retention on/in amorphous silica. Furthermore, Mg atoms are located at a distance indicating a bidentate binding mode because R_{Am-Mg1} would have been larger for monodentate binding: the upper limit for monodentate binding is $R_{Am-O1} + R_{O-Mg1} = 2.42 + 2.08 = 4.50$ Å. In that configuration, the

Table 2
Quantitative EXAFS analysis of higher distances atomic shells[a].

AmCopBru

Angle (α)	Mg1 shell			Mg2 shell			O2 shell			O3 shell		
	N	*R*	σ^2	*N*	*R*	σ^2	*N*	*R*	σ^2	*N*	*R*	σ^2
10°	1.8			1.6(3)			3.0			2.4		
35°	2.4(3)	3.24	0.004	2.9	3.48	0.004	3.3(7)	3.87	0.004	1.6(1.0)	4.38(2)	0.004
80°	1.7			1.5			1.8(5)			2.2(8)		

AmCopHec

Angle (α)	Mg1 shell			Si1 shell			O2 shell		
	N	*R*	σ^2	*N*	*R*	σ^2	*N*	*R*	σ^2
35°	1.9(3)	3.17	0.008	1.0	3.33(3)	0.007	2.0	3.71	0.006

AmAdsHec

Angle (α)	Mg1 shell			Si1 shell			O2 shell		
	N	*R*	σ^2	*N*	*R*	σ^2	*N*	*R*	σ^2
35°	1.8(7)	3.22	0.006	0.9	3.38	0.004	0.3	3.79	0.006

N is the coordination number, *R* is the interatomic distance [Å], and σ^2 is the mean square displacement [$Å^2$]. The number in parentheses indicates the uncertainty, otherwise parameter held fixed.

[a] The data were fit over the entire range considering all shells from Tables 1 and 2.

number of neighboring Mg and Si is limited, in agreement with fit results (1 2 Mg and <1 Si atoms). The O_2 shell detected at higher distance also has a low coordination number, as could be expected for a surface sorbed species. This shell significantly differs from that detected in the coprecipitation sample.

The present data indicate that monomeric inner sphere surface complexes are formed upon surface adsorption of Am onto hectorite. This species is singularly different from that obtained by coprecipitation, meaning that only a marginal amount of surface sorbed Am may be present in AmCopHec.

3.3. Relevance with regard to HLW disposal and natural systems

HLW glass corrosion experiments performed in the laboratory showed evidence for the formation of various secondary phases that can possibly retain the RN leached out of the corroding waste matrix either by structural incorporation and/or by surface adsorption. The presence of Mg in the clayey groundwater was found to favor the formation of magnesium silicates phases (Jollivet et al., 2012), and the magnesium smectite hectorite is taken here as model system. In the glass alteration layer, RN structural incorporation is very likely because they are present in the aqueous environment during the formation of corrosion phases from the early stage (i.e., nucleation). It is also anticipated that the presence of An(III) will lead to large lattice strains and locally distort the octahedral site. Thus, low crystalline domains surrounding the incorporated cation may form and be randomly distributed in the bulk crystalline smectite. Consequently, it is also very likely that the actinide may be released at a rate higher than other octahedral cations upon clay leaching. However, geochemical conditions such as the expected presence of dissolved silica due to glass corrosion may also inhibit the clay destabilization, and thus the An(III) release.

Surface adsorption obviously occurs when RNs are in contact with the pre formed secondary phase or when the RN cannot enter the bulk structure during crystal growth. Compared to incorporation, the re mobilization of An(III) surface sorbed can be expected to be easier. Earlier works showed that the formation of surface complexes is reversible, meaning that a change in the chemical conditions, such as a decrease in pH (e.g., (Rabung et al., 2005)), will lead to a re mobilization of the actinides bound at mineral surfaces. Giving this, assuming that RN will only be retained at mineral surfaces in deep repositories will probably result in underestimating the retention potential of neo formed corrosion phases.

Numerous studies dedicated to the structural characterization of metal ions retained at the surface of smectites have been published over the past decades. Different uptake mechanisms, depending on geochemical conditions, have been identified. For example, Co(II), Ni(II) and Zn(II) form inner sphere surface complexes at the platelet edge sites (Schlegel et al., 2001b; Schlegel et al., 1999c; Dähn et al., 2003). Furthermore, the presence of dissolved silica has been shown to promote the epitaxial growth (Schlegel et al., 2001a; Dähn et al., 2002), meaning that the cation present in solution is first retained at the surface before it becomes structurally incorporated with increasing reaction time. Finally, laboratory experiments have also demonstrated the formation of trioctahedral clay minerals as coating on silicates, and these neoformed clays were able to retain metal ions in their bulk structure (Manceau et al., 1999). All these retention mechanisms have important impacts on the availability of metal ions. Additionally, the presence of sorbed metal ions at the edge sites also has an influence on the clay stability. For example, the presence of Co(II) at the solid/liquid interface drastically inhibits the lability of protonated Mg octahedra located at the platelet edges, thus inhibiting hectorite dissolution (Schlegel et al., 1999a).

Similar retention mechanisms and impact on sorbent stability can in principle also operate for RN in deep disposal sites. For example, like transition metal ions, the actinides Am or Cm form inner sphere surface complexes upon interaction with clay minerals in suspension (Geckeis et al., 2013). Because clay octahedral sheets are able to accommodate divalent and trivalent cations of large sizes, such as Cd(II) (Spagnuolo et al., 2004) or Lu(III) (Finck et al., 2009), the size (up to a certain limit) and the charge of the incorporated cation are not limiting factors. The structural incorporation of An(III) may not only result from coprecipitation, but surface retention followed by epitaxial growth may also lead to actinides located within a clay like structure. Finally, incorporation of An(III) ions into the crystal lattice may also take place by an entrapment mechanism as proposed e.g. by Heberling et al. (2014). In this case, precipitation kinetics and the degree of solid phase oversaturation play imperative roles. These mechanisms are not restricted to actinides, but may operate as well for all heavy metal ions present in the environment. This is supported by the presence of trace amounts of various cations in naturally occurring sheet silicates.

4. Conclusion

For the first time, hectorite was crystallized from a brucite precursor phase that was precipitated in the presence of Am(III). XRD and SEM data show that the actinide had no significant influence on the smectite multi step synthesis mechanism. XAS data indicate that Am(III) is sequentially occluded in distinct environments, from an octahedral brucite like to an octahedral clay like environment. Furthermore, the lack of angular dependence on the P EXAFS data collected for the precursor and the low coordination numbers of the cationic shells in brucite and hectorite suggest an occlusion in a strained lattice site, as a consequence of the substitution by the large Am ion. Obviously, trivalent actinides can be incorporated in clay minerals, but the structural compatibility is highly limited, as indicated by their release during clay crystallization. In contrast, Am(III) forms monomeric inner sphere surface complexes at the platelet edges upon surface retention. Depending on the sample preparation mode, Am is located at structurally distinct sites. There was no evidence of surface complexes during clay crystallization and no sample contained Am precipitated as a separate phase or bound to an X ray amorphous phase.

The results of this study shed new light on the possible trivalent actinide incorporation pathway in sheet silicates in low temperature aqueous environments. The formation of clay minerals as secondary phases upon HLW glass matrix dissolution and subsequent re precipitation in the presence of actinides can in principle represent a very efficient retention mode. Such information is of high importance in safety assessment calculations of deep nuclear waste repositories.

Because of their large sizes, the actinides very likely have to be taken up in a less constrained octahedral environment in a precursor phase (such as brucite) to be incorporated in a more constrained clay like environment. However, the compatibility for An(III) at structural sites is very limited and localized clay like precipitates very likely form in the actinide vicinity as a consequence of local deformation. Such domains may certainly be randomly distributed and thus have only limited impact on the bulk clay formation and crystallinity. Yet, the lack of short range crystallinity may possibly have an impact on the long term stability of the retention because the stability of such domains certainly differs from that of the bulk phase. This will in turn have implications for the long term RN mobilization/immobilization. Further investigations are needed to address this point.

Acknowledgments

The synchrotron light source ANKA is acknowledged for provision of synchrotron radiation beam time. Eva Soballa (KIT INE) is thanked for the collection of SEM data. The radioprotection officers of KIT INE are thanked for their assistance. Comments by anonymous reviewers and the editor are acknowledged.

Appendix A

The fit quality was quantified by the R_f factor (Ravel, 2000) representing the absolute misfit between theory and experimental data:

$$R_f \quad \frac{\sum_{i\ \ 1}^{N} \left\{ [Re(f_i)]^2 + [Im(f_i)]^2 \right\}}{\sum_{i\ \ 1}^{N} \left\{ [Re(FT_{data}(P_i))]^2 + [Im(FT_{data}(P_i))]^2 \right\}}$$

where $Re(f_i)$ and $Im(f_i)$ are the real and imaginary parts of the differ ence function $f_i = [FT_{data}(P_i) - FT_{model}(P_i)]$, $FT_{data}(P_i)$ and $FT_{model}(P_i)$ are the FT functions of the experimental data and the model, and the summation runs over all P_i values of the fitted $R + \Delta R$ range.

References

Ankudinov, A.L., Ravel, B., Rehr, J.J., Conradson, S.D., 1998. Real-space multiple-scattering calculation and interpretation of x-ray-absorption near-edge structure. Phys. Rev. B 58 (12), 7565–7576.

Bradbury, M.H., Baeyens, B., 2002. Sorption of Eu on Na- and Ca-montmorillonites: experimental investigations and modelling with cation exchange and surface complexation. Geochim. Cosmochim. Acta 66 (13), 2325–2334.

Brandt, H., Bosbach, D., Panak, P.J., Fanghanel, T., 2007. Structural incorporation of Cm(III) in trioctahedral smectite hectorite: a time-resolved laser fluorescence spectroscopy (TRLFS) study. Geochim. Cosmochim. Acta 71 (1), 145–154.

Catti, M., Ferraris, G., Hull, S., Pavese, A., 1995. Static compression and H-disorder in brucite, Mg(OH)(2), to 11 GPA—a powder neutron-diffraction study. Phys. Chem. Miner. 22 (3), 200–206.

Dähn, R., et al., 2002. Neoformation of Ni phyllosilicate upon Ni uptake on montmorillonite: a kinetics study by powder and polarized extended X-ray absorption fine structure spectroscopy. Geochim. Cosmochim. Acta 66 (13), 2335–2347.

Dähn, R., et al., 2003. Structural evidence for the sorption of Ni(II) atoms on the edges of montmorillonite clay minerals: a polarized X-ray absorption fine structure study. Geochim. Cosmochim. Acta 67 (1), 1–15.

Finck, N., Stumpf, T., Walther, C., Bosbach, D., 2008. TRLFS characterization of Eu(III)-doped synthetic organo-hectorite. J. Contam. Hydrol. 102 (3-4), 253–262.

Finck, N., Schlegel, M.L., Bosbach, D., 2009. Sites of Lu(III) sorbed to and coprecipitated with hectorite. Environ. Sci. Technol. 43 (23), 8807–8812.

Gates, W.P., Bouazza, A., Churchman, G.J., 2009. Bentonite clay keeps pollutants at bay. Elements 5 (2), 105–110.

Gaucher, E.C., et al., 2006. Modelling the porewater chemistry of the Callovian–Oxfordian formation at a regional scale. Compt. Rendus Geosci. 338 (12-13), 917–930.

Geckeis, H., Lützenkirchen, J., Polly, R., Rabung, T., Schmidt, M., 2013. Mineral–water interface reactions of actinides. Chem. Rev. 113 (2), 1016–1062.

Heberling, F., et al., 2014. A thermodynamic adsorption/entrapment model for selenium(IV) coprecipitation with calcite. Geochim. Cosmochim. Acta 134, 16–38.

Jollivet, P., et al., 2012. Effect of clayey groundwater on the dissolution rate of the simulated nuclear waste glass SON68. J. Nucl. Mater. 420 (1-3), 508–518.

Manceau, A., Schlegel, M., Nagy, K.L., Charlet, L., 1999. Evidence for the formation of trioctahedral clay upon sorption of Co2+ on quartz. J. Colloid Interface Sci. 220 (2), 181–197.

Meunier, A., 2005. Clays. Springer.

Pauling, L., 1929. The principles determining the structure of complex ionic crystals. J. Am. Chem. Soc. 51 (4), 1010–1026.

Polly, R., et al., 2010. Quantum chemical study of inner-sphere complexes of trivalent lanthanide and actinide ions on the corundum (0001) surface. Radiochim. Acta 98 (9-11), 627–634.

Rabung, T., et al., 2005. Sorption of Eu(III)/Cm(III) on Ca-montmorillonite and Na-illite. Part 1: Batch sorption and time-resolved laser fluorescence spectroscopy experiments. Geochim. Cosmochim. Acta 69 (23), 5393–5402.

Ravel, B., 2000. EXAFS analysis with FEFF and FEFFIT. Part 2: Commentary. Version 0.04.

Ravel, B., Newville, M., 2005. ATHENA, ARTEMIS, HEPHAESTUS: data analysis for X-ray absorption spectroscopy using IFEFFIT. J. Synchrotron Radiat. 12, 537–541.

Rothe, J., et al., 2012. The INE-beamline for actinide science at ANKA. Rev. Sci. Instrum. 83 (4).

Schlegel, M.L., Charlet, L., Manceau, A., 1999a. Sorption of metal ions on clay minerals: II. Mechanism of Co sorption on hectorite at high and low ionic strength and impact on the sorbent stability. J. Colloid Interface Sci. 220 (2), 392–405.

Schlegel, M.L., Manceau, A., Chateigner, D., Charlet, L., 1999b. Sorption of metal ions on clay minerals I. Polarized EXAFS evidence for the adsorption of Co on the edges of hectorite particles. J. Colloid Interface Sci. 215 (1), 140–158.

Schlegel, M.L., Manceau, A., Chateigner, D., Charlet, L., 1999c. Sorption of metal ions on clay minerals: I. Polarized EXAFS evidence for the adsorption of Co on the edges of hectorite particles. J. Colloid Interface Sci. 215 (1), 140–158.

Schlegel, M.L., Manceau, A., Charlet, L., Hazemann, J.L., 2001a. Adsorption mechanisms of Zn on hectorite as a function of time, pH, and ionic strength. Am. J. Sci. 301 (9), 798–830.

Schlegel, M.L., Manceau, A., Charlet, L., Chateigner, D., Hazemann, J.-L., 2001b. Sorption of metal ions on clay minerals. III. Nucleation and epitaxial growth of Zn phyllosilicate on the edges of hectorite. Geochim. Cosmochim. Acta 65 (22), 4155–4170.

Seidl, W., Breu, J., 2005. Single crystal structure refinement of tetramethylammonium-hectorite. Z. Krist. 220 (2-3), 169–176.

Severmann, S., Mills, R.A., Palmer, M.R., Fallick, A.E., 2004. The origin of clay minerals in active and relict hydrothermal deposits. Geochim. Cosmochim. Acta 68 (1), 73–88.

Shannon, R.D., 1976. Revised effective ionic radii and systematic studies of interatomic distances in halides and chalcogenides. Acta Crystallogr. A 32 (5), 751–767.

Skerencak-Frech, A., Frohlich, D.R., Rothe, J., Dardenne, K., Panak, P.J., 2014. Combined time-resolved laser fluorescence spectroscopy and extended X-ray absorption fine structure spectroscopy study on the complexation of trivalent actinides with chloride at T = 25–200 degrees C. Inorg. Chem. 53 (2), 1062–1069.

Spagnuolo, M., et al., 2004. Coprecipitation of trace metal ions during the synthesis of hectorite. Appl. Clay Sci. 27 (3–4), 129–140.

Stumpf, T., Hennig, C., Bauer, A., Denecke, M.A., Fanghanel, T., 2004. An EXAFS and TRLFS study of the sorption of trivalent actinides onto smectite and kaolinite. Radiochim. Acta 92 (3), 133–138.

Zimmer, P., Bohnert, E., Bosbach, D., Kim, J.I., Althaus, E., 2002. Formation of secondary phases after long-term corrosion of simulated HLW glass in brine solutions at 190 degrees C. Radiochim. Acta 90 (9-11), 529–535.

Karlsruher Institut für Technologie

OPEN ACCESS

Repository KITopen

Dies ist ein Postprint/begutachtetes Manuskript.

Empfohlene Zitierung:

Finck, N.; Dardenne, K.; Geckeis, H.
Am(III) coprecipitation with and adsorption on the smectite hectorite
2015. Chemical geology, 409
doi: 10.554/IR/110102166

Zitierung der Originalveröffentlichung:

Finck, N.; Dardenne, K.; Geckeis, H.
Am(III) coprecipitation with and adsorption on the smectite hectorite
2015. Chemical geology, 409, 12–19.
doi:10.1016/j.chemgeo.2015.04.020

Lizenzinformationen: CC BY-NC-ND 4.0